ORIGINAL ARTICLE

Structure-based design of novel heterocycle-substituted ATDP analogs as non-nucleoside reverse transcriptase inhibitors with improved selectivity and solubility

Li-Min Zhao[a,b,c], Christophe Pannecouque[d], Erik De Clercq[d], Shuai Wang[b,c,*], Fen-Er Chen[a,b,c,*]

[a]*Key Laboratory of Natural Resources of Changbai Mountain & Functional Molecules, Ministry of Education, Yanbian University College of Pharmacy, Yanbian University, Yanji 133002, China*
[b]*Engineering Center of Catalysis and Synthesis for Chiral Molecules, Department of Chemistry, Fudan University, Shanghai 200433, China*
[c]*Shanghai Engineering Center of Industrial Asymmetric Catalysis for Chiral Drugs, Shanghai 200433, China*
[d]*Rega Institute for Medical Research, KU Leuven, Leuven B-3000, Belgium*

Abstract Following on our recently developed biphenyl-ATDP non-nucleoside reverse transcriptase inhibitor ZLM-66 (SI = 2019.80, S = 1.9 μg/mL), a series of novel heterocycle-substituted ATDP derivatives with significantly improved selectivity and solubility were identified by replacement of the biphenyl moiety of ZLM-66 with heterocyclic group with lower lipophilicity. Evidently, the representative analog **7w** in this series exhibited dramatically enhanced selectivity and solubility (SI = 12,497.73, S = 4472 μg/mL) in comparison with ZLM-66 (SI = 2019.80, S = 1.9 μg/mL). This new NNRTI conferred low nanomolar inhibition of wild-type HIV-1 strain and tested mutant strains (K103N, L100I, Y181C, E138K, and K103N + Y181C). The analog also demonstrated favorable safety and pharmacokinetic profiles, as evidenced by its insensitivity to CYP and hERG, lack of mortality and pathological damage, and good oral bioavailability in rats (F = 27.1%). Further development of **7w** for HIV therapy will be facilitated by this valuable information.

*Corresponding authors.

E-mail addresses: shuaiwang@fudan.edu.cn (Shuai Wang), rfchen@fudan.edu.cn (Fen-Er Chen).

1. Introduction

Acquired immunodeficiency syndrome (AIDS), first identified in the United States in 1981, is an infection caused by human immunodeficiency virus type 1 (HIV-1)[1,2]. Despite significant advances in HIV treatment, the number of new infections and related deaths remains high. By the end of 2021, 38 million people worldwide were living with HIV. There were an estimated 1.5 million new infections and 650,000 AIDS-related deaths in 2021[3]. Reverse transcriptase (RT) is a key enzyme that is closely involved in the process of HIV replication[4]. Inhibition of RT leads to decreased viral load in patients, as shown with currently FDA-approved six non-nucleoside reverse transcriptase inhibitors (NNRTIs), including rilpivirine (RPV), etravirine (ETV), and doravirine (DOR), which effectively inhibit the synthesis of viral DNA along the RNA template by binding to an allosteric pocket[5,6]. However, a single amino acid mutation of RT enzyme may easily lead to a significant loss of efficacy of clinically used NNRTIs[7]. Thus, new second-generation therapeutic agents with broader mutant coverage and improved pharmaceutical profile are eagerly awaited.

Over the course of the last two decades, various strategies have been applied by us to seek structurally distinct, best-in-class NNRTIs[8–12]. A batch of new biphenyl-containing aryl triazolone dihydropyridine (ATDP) analogs were recently synthesized and identified as potent inhibitors of HIV RT[13]. Some of these analogs had nanomolar inhibition of WT HIV-1 and tested mutants. Within this series, the related pyridone ZLM-66 (2) in particular not only conferred exceptional potency against wild-type (WT) HIV-1 (EC_{50} = 13 nmol/L) but also had favorable activity against mutants, as shown in Fig. 1. The compound in question exhibited limited selectivity (SI = 2019.80) and inadequate aqueous solubility (S = 1.9 µg/mL, pH = 2.0), thereby impeding its potential for further advancement.

The objective of this investigation was to devise advanced NNRTIs that possess enhanced selectivity and aqueous solubility in comparison to ZLM-66. Quinoline or pyridine substituents, which exhibit high-water solubility, complex electrical effects, and unique metabolic pathways, are commonly utilized in drug design[14]. The inclusion of quinoline or pyridine substituents has been demonstrated to enhance the selectivity and drug-like characteristics of the primary compound[15,16]. Thus, a fragment-hopping approach was employed to replace the biphenyl ring of ZLM-66 with hydrophilic heterocyclic quinoline or pyridine substituents, with the expectation of enhancing its physicochemical properties and selectivity without compromising its anti-HIV activity (Fig. 2). The proposed approach was buttressed by anticipated outcomes, which suggested that the substitution of the biphenyl moiety of ZLM-66 with a quinoline substituent would confer advantages in terms of its safety and selectivity, as evidenced by Table S1. The aqueous solubility of 7w was remarkably
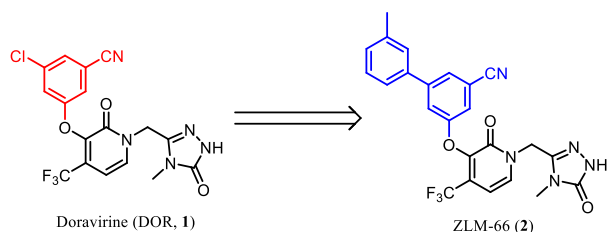
improved with a logP value of 0.59, lower than that of ZLM-66 (logP = 3.12). Furthermore, the molecule 7w was effectively positioned within the active pocket, exhibiting a comparable conformation to ZLM-66, as depicted in Fig. 2. The quinoline ring of 7w was directed towards the aromatic region, thereby establishing five aryl−aryl stacking interactions with W229 and Y188, as illustrated in Fig. 2B. In order to validate our supposition, a sequence of innovative heterocyclic-ATDPs were synthesized and subsequently assessed for their anti-HIV-1 effectiveness.

2. Results and discussion

2.1. Chemistry

The synthetic route to the targeted ATDPs 7a−7am is depicted in Scheme 1. Aryl nucleophilic substitution (ArSN) of the commercially available chloropyridine 3 with the appropriate phenols in the presence of anhydrous K_2CO_3 at 80 °C for 5 h proceeded smoothly in dry NMP with full conversion, leading to the corresponding biaryl ethers 4a−4am without isolation and purification, which was subjected to hydroxylation reaction by treating NaOH powder in t-BuOH at 70 °C for 8 h to afford the expected hydroxypyridine 5a−5am in 26%−67% yields. Ultimately, treatment of 5a−5am with chloromethyl triazolone (6) under Ducharme's conditions (anhydrous K_2CO_3, dry DMF, −10 °C, 30 min) resulted in the desired target molecules 7a−7am in 40%−78% yields[17,18].

2.2. Anti-HIV-1 activity

The antiviral activity and cytotoxicity of the newly synthesized compounds 7a−7am were assessed in MT-4 cells infected with HIV-1. The biological outcomes have been presented in Table 1, where the EC_{50} (anti-HIV efficacy), CC_{50} (cytotoxicity), and SI (selectivity index, CC_{50}/EC_{50} ratio) have been utilized as measures. During the course of this program, an extensive structure−activity relationship (SAR) was conducted, and the anti-HIV-1 potency of 39 new analogs and cytotoxicity were assessed in cellular assays using standard procedures. Reference data for ETR and DOR were included for comparison. The resultant data were organized in Table 1. Initially, the new molecules 7a−7t containing different pyridine or pyrimidine groups were synthesized by heterocyclic substitution of a biphenyl group of ZLM-66. The resulting biological data revealed that among these analogs, only 7a, 7e, and 7h retained nanomolar activity with EC_{50} values of 0.49−0.55 nmol/L, below that of ZLM-66 (EC_{50} = 13 nmol/L). The specific structure-activity relationship was as follows: the activity of compound 7a was significantly reduced (EC_{50} = 550 nmol/L) by the introduction of a m-chloropyridine substituent at the biphenyl ring site of ZLM-66. When transferring the chlorine substituent to an adjacent site of the nitrogen substituent resulted in further loss of potency (7b and 7c). By introducing an additional chlorine atom to the pyridine group of 7c, 7d was obtained, with a 17-fold increase in activity. The chlorine substituent of 7a or 7b was replaced by a bromine substituent, respectively, to obtain 7e or 7f, with no significant change in activity. However, the replacement of the chlorine substituent of 7c led to a significant loss of potency (7g, EC_{50} = 196.79 µmol/L). The analogs 7h, 7i, and 7j were designed by the substitution of the chlorine substituent of 7a, 7b, and 7c, respectively, which proved to be almost equipotent to that of the corresponding parent

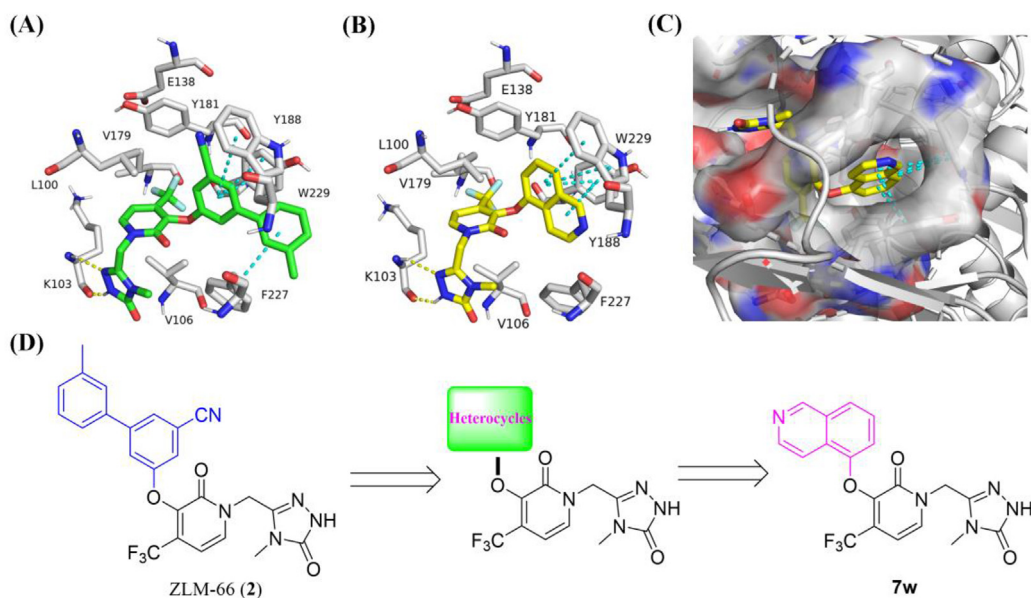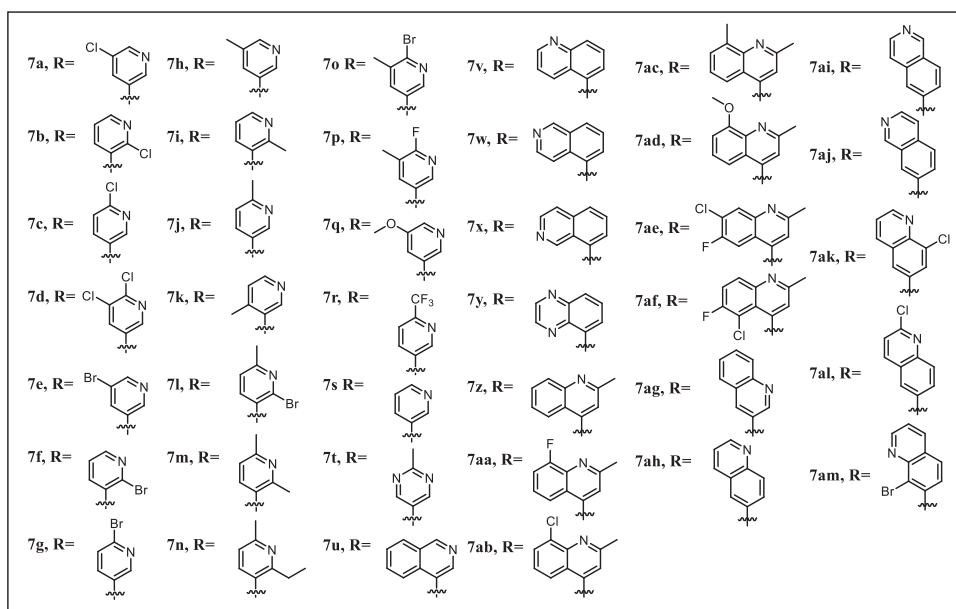**Figure 1** The discovery of ZLM-66.

Figure 2 (A) Rendering of ZLM-66 with WT RT (PDB code: 4NCG); (B−C) Molecular docking of **7w** with RT; (D) Structure-based design of novel heterocycle-ATDPs.
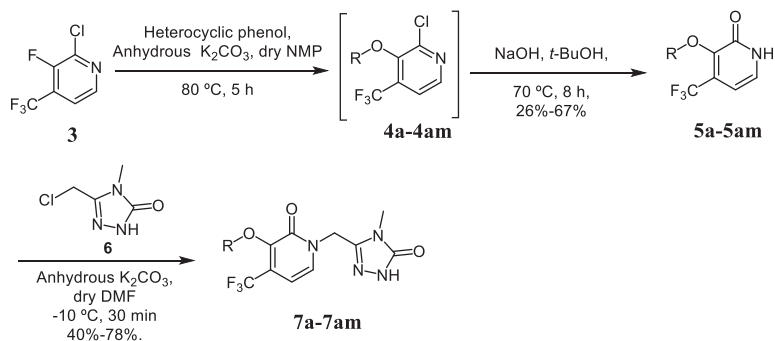
Scheme 1 Synthesis of ATDPs **7a−7am**.

Table 1 Anti-HIV-1 activity of ATDPs **7a−7t**.
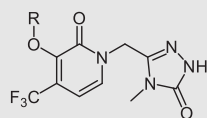
Compd.	R	EC$_{50}$[a] (μmol/L)	CC$_{50}$[b] (μmol/L)	SI[c]
7a		0.55 ± 0.23	>311	>563
7b		4.27 ± 0.75	289.90 ± 24.05	67.97
7c		35.57 ± 10.31	>311	>9
7d		2.02 ± 0.88	248.23 ± 28.17	122.98
7e		0.49 ± 0.12	>280	>573
7f		4.44 ± 0.94	270.85 ± 1.77	61.07
7g		196.79 ± 58.87	>280	>1
7h		0.53 ± 0.16	>328	>616
7i		6.76 ± 1.07	>328	>49
7j		21.14 ± 5.0	>328	>49
7k		1.53 ± 0.25	>328	>214
7l		>250	252.59 ± 16.75	<1
7m		>250	>250	<1
7n		>250	299.19 ± 3.74	1
7o		1.27 ± 0.36	>272	>214
7p		1.46 ± 0.54	>250	>214
7q		7.33 ± 5.03	>250	>43
7r		>250	>250	>1
7s		1.22 ± 0.24	>367	>278
7t		>250	>250	>1
ZLM-66	—	0.013 ± 0.0034	26.45 ± 2.42	2019.80

(continued on next page)

Table 1 (*continued*)

Compd.	R	EC$_{50}$[a] (µmol/L)	CC$_{50}$[b] (µmol/L)	SI[c]
DOR	—	0.013 ± 0.004	293.24 ± 0.17	22,556.92
ETR	—	0.0029 ± 0.002	>4.60	>1600

[a]EC$_{50}$: concentration of compound required to achieve 50% protection of MT-4 cell cultures against HIV-1-induced cytotoxicity, as determined by the MTT method, and values are the mean ± SD of at least two parallel tests.

[b]CC$_{50}$: concentration required to reduce the viability of mock-infected cell cultures by 50%, as determined by the MTT method, and values were averaged from at least four independent experiments.

[c]SI: selectivity index, the ratio of CC$_{50}$/EC$_{50}$.

Table 2　　Anti-HIV-1 efficacy of **7u−7am.**

Compd.	R	EC$_{50}$[a] (µmol/L)	CC$_{50}$[b] (µmol/L)	SI[c]
7u		0.89 ± 0.23	276.6 ± 10.08	309.52
7v		4.48 ± 1.24	278.33 ± 18.59	62.10
7w		0.022 ± 0.01	273.95 ± 10.56	12,497.73
7x		1.23 ± 0.28	>299	>244
7y		8.07 ± 1.41	220.30 ± 35.48	27.30
7z		>233	233.26 ± 32.085	<1
7aa		>220.31	220.31 ± 44.35	<1
7ab		>232.67	232.67 ± 26.13	<1
7ac		>151.44	151.44 ± 27.93	<1
7ad		>244.18	244.18 ± 13.78	<1
7ae		11.73 ± 9.10	92.86 ± 43.99	7.92
7af		33.26 ± 9.61	81.53 ± 11.72	2.45
7ag		>250	>250	>1
7ah		251.59 ± 5.75	>299	>1
7ai		11.15 ± 2.83	>299	>27
7aj		20.53 ± 8.02	>299	>15
7ak		>192.06	192.06 ± 42.91	<1
7al		46.69 ± 12.48	171.6 ± 44.92	3.68
7am		>163.98	163.98 ± 25.49	<1

Table 2 (*continued*)

Compd.	R	EC_{50}[a] (μmol/L)	CC_{50}[b] (μmol/L)	SI[c]
ZLM-66	–	0.013 ± 0.0034	26.45 ± 2.42	2019.80
DOR	–	0.013 ± 0.004	293.24 ± 0.17	22,556.92
ETR	–	0.0029 ± 0.002	>4.60	>1600

[a]EC_{50}: concentration of compound required to achieve 50% protection of MT-4 cell cultures against HIV-1-induced cytotoxicity, as determined by the MTT method, and values are the mean ± SD of at least two parallel tests.
[b]CC_{50}: concentration required to reduce the viability of mock-infected cell cultures by 50%, as determined by the MTT method, and values were averaged from at least four independent experiments.
[c]SI: selectivity index, the ratio of CC_{50}/EC_{50}.

compound against the MT-4 HIV-1 WT strain. Transferring the methyl group of **7j** to the nitrogen counterpart yielded **7k**, being 14-fold more potent than **7j**. Incorporation of bromine, methyl, or ethyl group into the pyridine of **7j** caused considerable decrease of activity with EC_{50} exceeding 250 μmol/L. Similarly, adding a bromide or fluorine substituent to the pyridine of **7h** decreased its activity (**7o** and **7p**). The substitution of the chlorine substituent in **7a** with a methoxy group decreased the activity (**7q**, EC_{50} = 7.33 μmol/L). Introduction of a trifluoromethyl

substituent to replace the chlorine substituent of **7c** caused a complete loss of activity (**7r**, EC_{50} > 250 μmol/L). Removal of the chlorine group of **7a** afforded **7s**, which showed moderate inhibition of WT HIV-1 (EC_{50} = 1.22 μmol/L). In addition, an attempt was made to incorporate an additional nitrogen substituent into the pyridine groups of **7j**, which was unfortunately ineffective against WT HIV-1 (EC_{50} > 250 μmol/L). It was worth noting that the cytotoxicity of these compounds was very low, all of which were greater than 248 μmol/L.
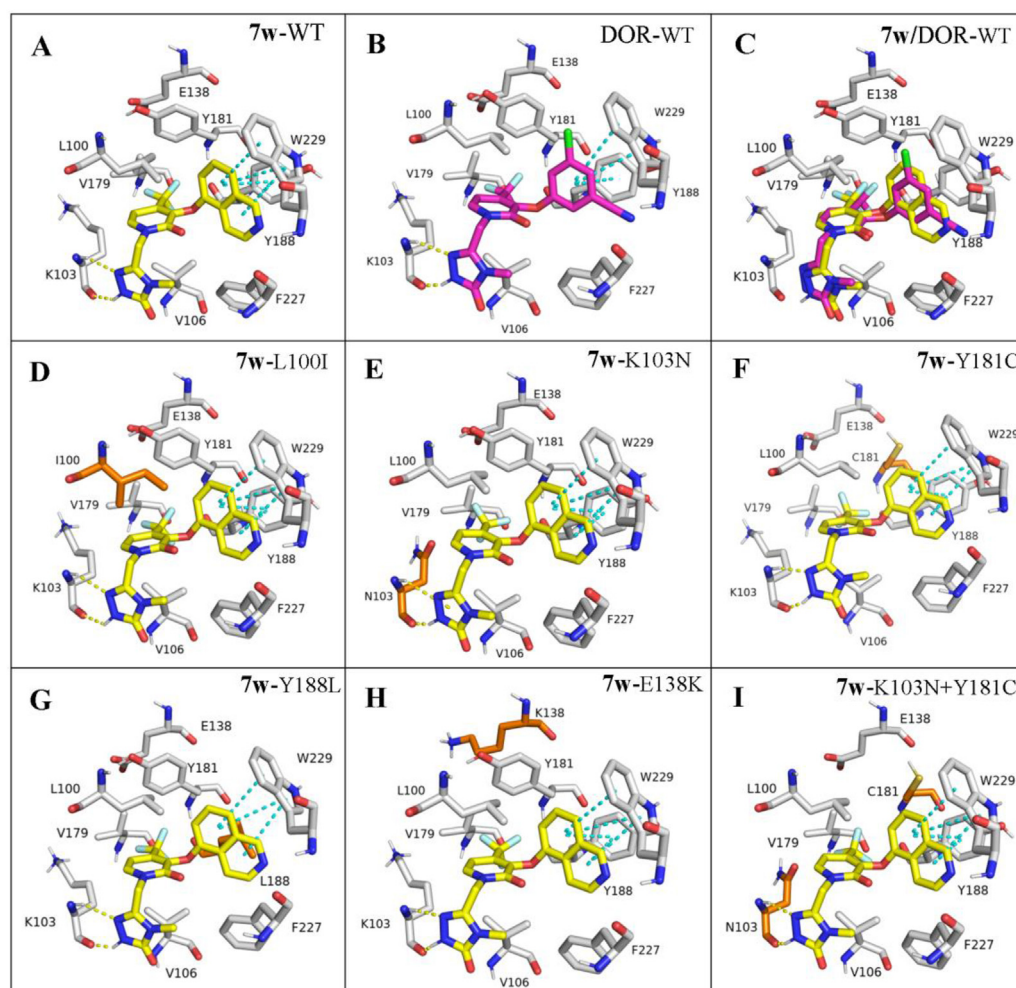

Figure 3 Molecular docking of **7w** (yellow) and DOR (purple) with RT and mutants (PDB code: 4NCG).

Table 3   Anti-HIV-1 efficacy of representative analogs against mutants.

Compd.	EC$_{50}$ (μmol/L)[a]					
	L100I	K103N	Y181C	Y188L	E138K	K103N + Y181C
7a	0.93 ± 0.51	1.22 ± 0.56	1.79 ± 0.58	122.05 ± 62.08	0.61 ± 0.04	18.34 ± 11.44
7e	0.68 ± 0.22	0.95 ± 0.27	0.85 ± 0.15	39.01 ± 5.33	0.62 ± 0.22	12.28 ± 8.12
7h	0.55 ± 0.33	1.20 ± 0.18	1.78 ± 0.10	196.28 ± 12.06	0.77 ± 0.04	16.11 ± 7.33
7u	0.50 ± 0.22	3.01 ± 1.42	1.56 ± 0.49	>250	0.90 ± 0.29	33.99 ± 13.04
7w	0.038 ± 0.017	0.071 ± 0.019	0.050 ± 0.011	5.35 ± 2.15	0.049 ± 0.013	0.14 ± 0.09
ZLM-66	0.024 ± 0.0049	0.013 ± 0.0026	0.058 ± 0.021	0.76 ± 0.13	0.025 ± 0.0033	0.26 ± 0.12
DOR	0.0066 ± 0.0017	0.042 ± 0.0013	0.025 ± 0.0023	0.50 ± 0.15	0.0075 ± 0.0026	0.142 ± 0.057
ETR	0.006 ± 0.004	0.002 ± 0.000	0.019 ± 0.009	0.018 ± 0.008	0.006 ± 0.001	0.031 ± 0.009

[a]EC$_{50}$: The effective concentration required to protect MT-4 cells against viral cytopathicity by 50%, and values were averaged from at least three independent experiments.

Table 4   Effect of representative analogs on RT.

Compd.	IC$_{50}$ (μmol/L)	Compd.	IC$_{50}$ (μmol/L)
7a	1.14 ± 0.043	ZLM-66	0.041 ± 0.0044
7e	0.74 ± 0.03	**7w**	0.12 ± 0.007
7h	1.03 ± 0.14	DOR	0.044 ± 0.005
7u	4.38 ± 0.35		

To identify privileged segments of HIV-1 RT inhibition, we next turn our attention to structurally distinct quinoline substituents, as described in Table 2. Results revealed that compound **7w** proved to be a very strong inhibitor of WT HIV-1 (EC$_{50}$ = 22 nmol/L) that was as potent as DOR and ZLM-66 in the cellular assay of MT-4. The nitrogen of the quinoline of **7w** closely mimicked the nitrogen at the position of the cyano group in DOR, thus displaying a good EC$_{50}$ value, as shown in
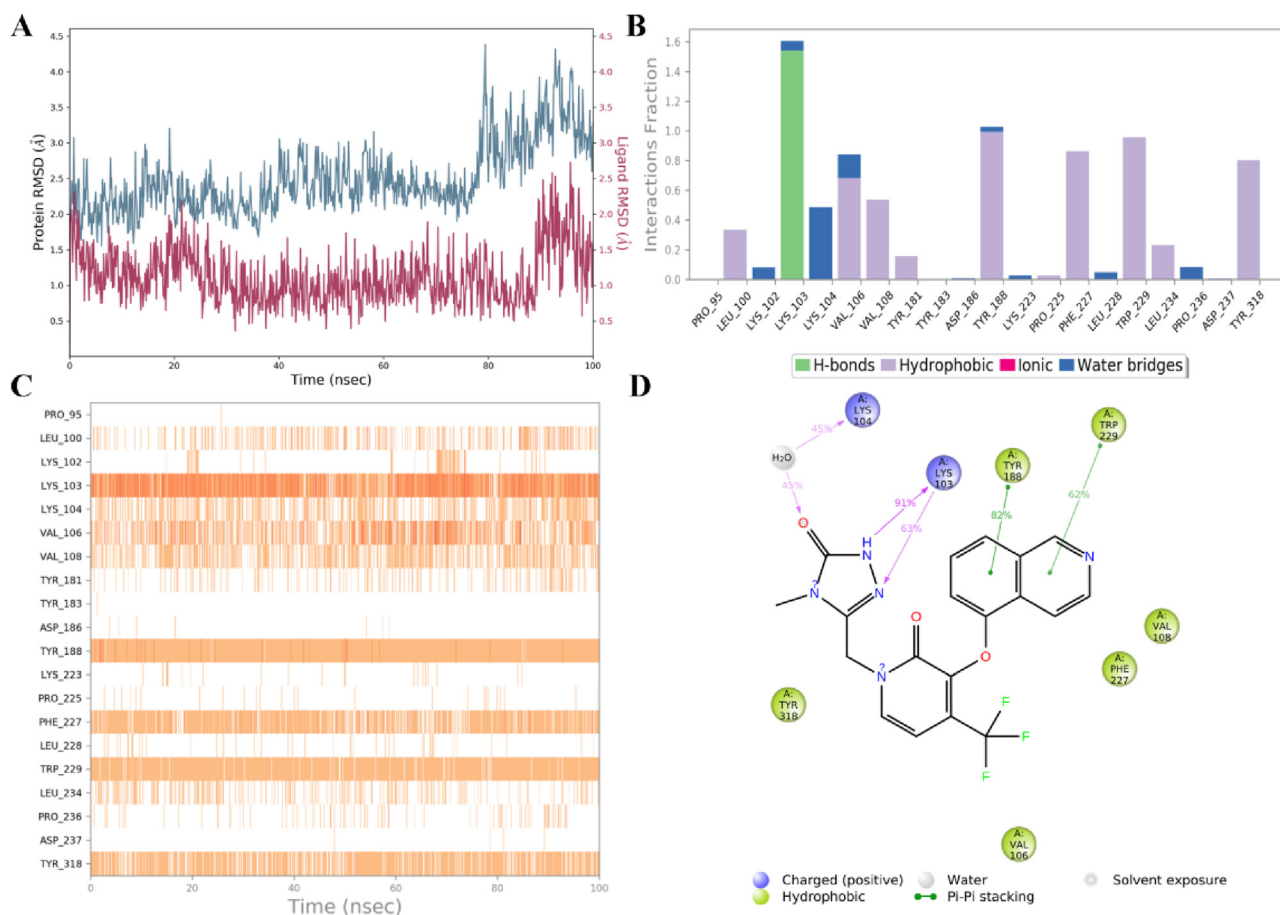

Figure 4   Molecular dynamic simulations of **7w** with WT RT (PDB code: 4NCG).

Table 5 Aqueous solubility of **7w**.

Compd.	pH = 7.0 (µg/mL)	pH = 7.4 (µg/mL)	pH = 2.0 (µg/mL)
7w	38	53	4472
ZLM-66	—	—	1.9
DOR	19	—	—

Table 6 Effect of **7w** on CYP isoforms.

CYP subtypes	Reference drug	IC_{50} (µmol/L)	Compd.	IC_{50} (µmol/L)
CYP1A2	Phenacetin	0.021	**7w**	>50
CYP2C19	Mephenytoin	2.42	**7w**	26.83
CYP2C9	Tolbutamide	0.832	**7w**	19.56
CYP2D6	Dextromethorphan	0.0482	**7w**	>50
CYP3A4-M	Midazolam	0.0713	**7w**	>50
CYP3A4-T	Testosterone	0.0436	**7w**	>50

Table 7 PK profiles of **7w** in rat.

Parameter	**7w**		ZLM-66[13]
	1.0 mg/kg (i.v.)	5.0 mg/kg (p.o.)	5.0 mg/kg (p.o.)
$t_{1/2}$ (h)	0.29 ± 0.21	1.79 ± 0.29	
T_{max} (h)	0.083 ± 0	0.417 ± 0.144	
C_{max} (ng/mL)	456 ± 51.1	2888 ± 9.71	
AUC_{0-t} (h·ng/mL)	229 ± 45.3	304 ± 24.5	
$AUC_{0-\infty}$ (h·ng/mL)	230 ± 46	312 ± 25.3	
MRT_{0-t} (h)	0.352 ± 0.0416	1.17 ± 0.153	
$MRT_{0-\infty}$ (h)	0.366 ± 0.467	1.42 ± 0.14	
F (%)		27.1 ± 0.0219	140.24

Fig. 3. Remarkably, the cytotoxicity of **7w** was greatly reduced with a high SI (CC_{50} = 273.95 µmol/L, SI = 12,497.73), which was obviously better than that of ZLM-66 (CC_{50} = 26.45 µmol/L, SI = 2019.80). The specific structure-activity relationship was as follows: introduction of a quinoline substituent at the site of the pyridine group in **7s** afforded **7u**, with a slightly increased activity (EC_{50} = 0.89 µmol/L). Variation of the nitrogen position of quinoline produced **7v**−**7x**, which surprisingly identified **7w** (EC_{50} = 22 nmol/L) as the most active compound in this series. Incorporation of an additional nitrogen substituent at the quinoline group of **7v** provided **7y**, and the potency was reduced by 2-fold. **7z**−**7af** were designed by adjusting the nitrogen position of quinoline ring and the change of different substituents, but only **7ae** and **7af** showed moderate inhibition against WT HIV-1. The conversion of quinoline junction site caused a dramatical drop in activity (**7ag**−**7am**). All these compounds except **7ae** and **7af** were characterized by low cytotoxicity.

2.3. Antiviral efficacy of representative analogs against mutant HIV-1

For selected five molecules that possessed high inhibition of WT HIV-1, data were collected against six mutant HIV-1 strains. Reference data for ZLM-66, ETR, and DOR were also included for comparison. As seen in Table 3, with the exception of Y188L, all of these compounds effectively inhibited HIV-1 mutants at the

nanomolar or low micromolar level. Compound **7w** was found to be the best inhibitor of the tested HIV-1 mutant strains, consistent with its inhibitory effect on WT HIV-1. The activity of **7w** was close to or slightly lower than that of DOR, but comparable to ZLM-66. Except Y188L, **7w** showed low nanomolar inhibitory activity against K103N, L100I, E138K, Y181C, and K103N + Y181C, with EC_{50} value in the range of 35−140 nmol/L. In the case of Y188L, **7w** exhibited moderate inhibitory activity (EC_{50} = 5.35 µmol/L), which was lower than that of ZLM-66 and DOR. In terms of K103N + Y181C, the activity of **7w** was comparable activity to DOR, which was superior to ZLM-66.

2.4. Anti-HIV-1 efficacy of representative analogs toward the WT HIV-1 RT

To confirm their target of the newly designed analogs, **7a**, **7e**, **7h**, **7u**, and **7w** that were active at the cellular level were tested for inhibition of WT HIV-1 RT compared with DOR and ZLM-66. The results were organized in Table 4. It was found that the tested analogs had good inhibition of WT HIV-1 RT, and especially, **7w** was identified as the most active inhibitor in this series (IC_{50} = 0.12 µmol/L), which was slightly less potent than DOR and ZLM-66. These findings confirmed that these agents suppressed the HIV-1 replication by targeting HIV-1 RT.

2.5. Molecular modeling

Modeling of **7w** with RT (PDB code: 4NCG) was performed using the software Glide SP to determine the binding style. Comparing the binding mode of **7w** with DOR indicated that **7w** bound
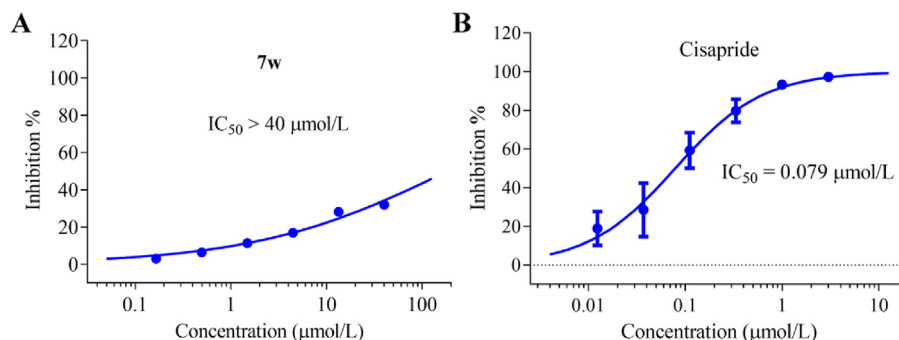
Figure 5 Effect of **7w** (A) and cisapride (B) on hERG.

identically to the protein, as described in Fig. 3A−C, which were packed with several classical hydrogen bonds and aryl−aryl interactions. The newly introduced quinoline moiety was located in the hydrophobic cleft composed of Y188, Y181, and W229, which was packed with π−π interactions with Y188 and W229. The nitrogen of the quinoline of **7w** closely mimicked the cyano group of DOR in the NNIBP of WT RT (Fig. 3C). The pyridone ring of **7w** conformationally restricted the directions of triazolone and quinoline in the binding pockets of NNIBP. Two hydrogen bonds between the triazolone moiety and the K103 were detected. In addition, **7w** fitted well into the mutant binding pockets, respectively, and several main interactions were also observed, as described in Fig. 3D−I. However, the low activity of Y188L was attributed to the absence of part of the π−π bonds, as depicted in Fig. 3I. Molecular docking for Y188L: compared with ZLM-66

and DOR, **7w** retained crucial hydrogen bonds and aryl−aryl interactions with neighboring residues, and displayed a docking score that was comparable to them as presented in Supporting Information Table S2. However, the inhibitory potency of **7w** against Y188L was comparatively inferior to that of ZLM-66 and DOR, thereby necessitating additional structural refinement.

2.6. Molecular dynamic simulations

Molecular docking simulations of **7w** were carried out by leveraging the previously reported computational protocol[19]. The results, as depicted in Fig. 4, demonstrated that **7w** maintained its original binding style with the protein throughout 100 ns due to the lower RMSD fluctuations of the ligand than protein, suggesting that the complex stabilized rapidly. A schematic diagram
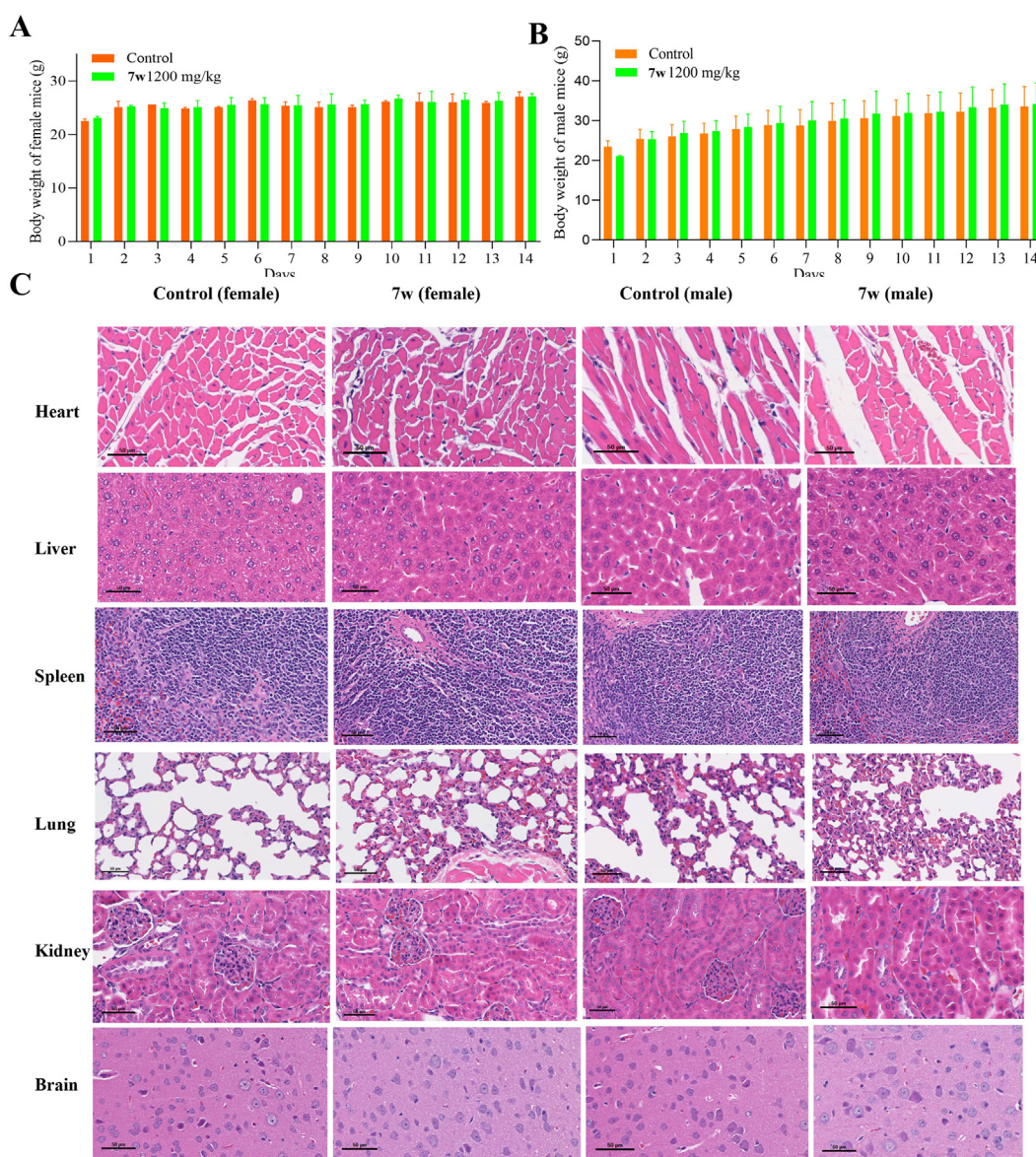

Figure 6 The effect of **7w** on body weight of female (A) and male (B) mice; (C) The effect of **7w** on six important organs (magnification: 200×; scale bar: 50 μm).

of the interaction between **7w** and protein was collected in Fig. 4B–D. Hydrogen bonds, hydrophobic bridges, ion bridges, and water bridges were included within 100 ns (Fig. 4B). Results indicated that the hydrophobic and aryl–aryl stacking interactions between **7w** and W229/Y188 persisted throughout the 100 ns (Fig. 4C and D). Hydrogen bonds of the ligand with K103 were found within 100 ns. A water bridge-mediated hydrogen bond was also detected between the ligand and K104.

2.7. Aqueous solubility

The aqueous solubility of **7w** was also determined in comparison with ZLM-66 and DOR at three different pH values, using the previously reported HPLC method[20]. As evidenced by the results in Table 5, **7w** exhibited better aqueous solubility than that of ZLM-66 and DOR at three different pH values. Especially, at a pH of 2.0, the solubility of **7w** was 4472, which was exceptionally superior to DOR and ZLM-66. These findings suggest that **7w** may have potential as a more effective therapeutic agent than its counterparts in certain pH environments.

2.8. CYP inhibitory activity

Drug–drug interactions are commonly attributed to the inhibition of CYP. FDA approved second-generation NNRTIs, RPV and ETR, were found to be potent CYP2C9 and CYP2C19 suppressants and CYP3A4 inducers[21,22]. It has been reported that CYP isoforms were not sensitive to ZLM-66 and DOR[13,23]. To mitigate the potential risks associated with drug interactions, it was decided to assess the effect of **7w** on CYP isoforms, and the results were organized in Table 6. Pleasingly, **7w** was not sensitive to CYP isoforms, even in the case of CYP2C19 and CYP2C9, where weak inhibition was observed, with IC_{50} values approaching or exceeding 20 μmol/L.

2.9. hERG inhibitory activity

Suppression of hERG is associated with cardiotoxicity[24]. It is highly recommended to conduct an early assessment of hERG toxicity[25]. Recent investigations have revealed that both ZLM-66 and DOR exhibited minimal inhibitory activity toward hERG[13,26]. To mitigate the potential risk of cardiotoxicity, the activity of **7w** against hERG was assayed in CHO-hERG cells, and cisapride was selected as the reference. Encouragingly, **7w** negligible impact on hERG ($IC_{50} > 40$ μmol/L), which was lower than cisapride, as described in Fig. 5.

2.10. Pharmacokinetics analysis

Building upon the aforementioned discoveries, we proceeded to assess the pharmacokinetic (PK) profiles of the most potent compound, **7w**, in Sprague–Dawley rats. Our results, as presented in Table 7, demonstrated that **7w** was endowed with good pharmacokinetic characteristics in rats. Upon intravenous administration, the half-life of **7w** was 0.29 h and the mean residence time was 0.352 h. The maximum concentration ($C_{max} = 456$ ng/mL) rapidly occurred after 0.083 h. Upon oral administration of 5.00 mg/kg, **7w** yielded a longer half-life ($t_{1/2} = 1.79$ h) and increased maximum concentration ($C_{max} = 2888$ ng/mL). Importantly, despite being

lower than the positive compound ZLM-66, **7w** maintained favorable oral bioavailability ($F = 27.1\%$).

2.11. Acute toxicity assay

An *in vivo* safety assessment of **7w** was conducted in rats through an acute toxicity assay. Intragastric administration of 1.2 g/kg **7w** did not result in any fatalities, as evidenced by Fig. 6A and B. Furthermore, mice treated with **7w** exhibited normal behavior and weight, with no observable abnormalities. The effect of **7w** on six main organs was also detected using HE staining, which revealed that **7w** caused no obvious pathological damage, as described in Fig. 6C. These results collectively indicate a favorable *in vivo* safety profile for **7w**.

3. Conclusions

In this work, we have synthesized a series of novel heterocycle-substituted ATDP analogs through a fragment-hopping approach aiming to facilitate the selectivity and solubility of ZLM-66 (SI = 2019.80, S = 1.9 μg/mL). This family of RT inhibitors was further assessed, which proved to have substantial benefits in terms of selectivity and solubility. This work led to the disclosure of the representative compound **7w**, which had greatly enhanced selectivity and solubility (SI = 12,497.73, S = 4472 μg/mL), superior to ZLM-66 (SI = 2019.80, S = 1.9 μg/mL). The new analog showed nanomolar inhibition of WT HIV-1 and common mutants. In addition, it possessed weak inhibition of CYP and hERG, good pharmacokinetics profiles, and favorable *in vivo* safety profile. Overall, encouraging results reported herein support further development of **7w** as a lead compound.

4. Experimental

4.1. Chemistry

Synthetic protocols were described in Supporting Information.

4.2. Anti-HIV-1 assay

Anti-HIV-1 efficacy was assessed by leveraging disclosed method[27].

4.3. Modeling and molecular dynamic simulations

Detailed method for modeling and molecular dynamic simulations were previously described[19].

4.4. hERG channel Qpatch assay

The inhibitory activity of test compounds on hERG potassium channels was tested in CHO-hERG cells, which were cultured in 175 cm^2 culture flasks. The prepared cell density was $2-5 \times 106$/ mL. The single-cell high-impedance sealing and whole-cell pattern formation processes are automatically completed by the Qpatch instrument. After acquiring whole-cell recording mode, cells were clamped at −80 mV. The voltage stimulation was applied every 15 s, recorded for 2 min, and the extracellular fluid was administered for 5 min, and then the administration process

was started. Each test concentration was given for 2.5 min starting from the lowest test concentration. After serial administration of all concentrations, 3 μmol/L cisapride was administered. Graph-Pad Prism 5.0 software was used to analyze the resultant data.

4.5. Cytochrome P450 inhibition assay

First, construct an incubation system in a 96-well plate, and each well was composed of 20 μL human liver microsomes (0.3 mg/mL), 50 μL test sample or control, and 20 μL probe substrate in 0.1 mmol/L Tris (pH = 7.4). The final volume of each well was 100 μL. After 10 min incubation at 37 °C, 10 μL NADPH was added to each well (1 mmol/L) to initiate the reaction, followed by 15 min incubation at 37 °C. Finally, the reaction was terminated by the addition of a mixture of acetonitrile and internal standards (propranolol, nadolol). The supernatant was analyzed by LC−MS/MS.

4.6. PK study

Select 6 SD rats with a body weight of 180−220 g, and divide them into two groups randomly. Preliminary proposed dosage concentration: 10 mg/kg for intragastric administration and 1 mg/kg for intravenous injection, fasting for 12 h before administration. Manual blood sampling was performed at the following time points after dosing: 0 (pre-dose), 5, 10, 20, 30, 40, 50, 60, 90, 120, 240, 360, 480, 720 min. Add heparin sodium anticoagulant to the blood sample, centrifuge to obtain plasma, and store it at −80 °C. Add more than 2 times of organic solvent (such as acetonitrile) to the sample for shaking and centrifugation. The supernatant was taken, blown dry with nitrogen, reconstituted, and an HPLC−MS/MS method was set up to determine the plasma concentration. Concentration-time data were analyzed using WinNonlin software, and standard pharmacokinetic parameters and bioavailability were calculated.

4.7. Acute toxicity assay

Acute toxicity experiments were carried out using a protocol approved by Fudan University (2023-HXX-08JZS). Eight ICR mice weighing 24−28 g, 4 males and 4 females, aged 5−6 weeks, were selected. Eight mice were divided into 4 groups randomly. After a single intragastric administration, the mice were continuously observed for 14 days, and the changes in body weight, behavior, and coat color of the mice were recorded respectively. After 14 days, all mice were euthanized and dissected, and kidney, lung, spleen, liver, heart, and brain were selected for HE staining to observe histological changes.

Author contributions

Li-Min Zhao completed the synthesis and structural confirmation. Erik De Clercq and Christophe Pannecouque completed the biological assessment. Shuai Wang and Li-Min Zhao conducted experiments to evaluate drug properties and molecular docking studies. All authors contributed to the writing of this article. Fen-Er Chen conceived the project and provided resources, supervision and financial assistance.

All authors critically evaluated the manuscript prior to submission.

Conflicts of interest

The authors declared no conflicts of interest.

Appendix A.   Supporting information

Supporting data to this article can be found online at https://doi.org/10.1016/j.apsb.2023.07.008.

References

1. Barré-Sinoussi F, Chermann JC, Rey F, Nugeyre MT, Chamaret S, Gruest J, et al. Isolation of a T-lymphotropic retrovirus from a patient at risk for acquired immune deficiency syndrome (AIDS). *Science* 1983;**220**:868−71.
2. Popovic M, Sarin PS, Robert-Gurroff M, Kalyanaraman VS, Mann D, Minowada J, et al. Isolation and transmission of human retrovirus. *Science* 1983;**219**:856−9.
3. Global HIV & AIDS Statistics—2022 fact sheet. Joint United Nations Programme on HIV/AIDS 2022:1−2. https://www.unaids.org/en/resources/fact-sheet.
4. de Béthune MP. Non-nucleoside reverse transcriptase inhibitors (NNRTIs), their discovery, development, and use in the treatment of HIV-1 infection: a review of the last 20 years (1989−2009). *Antivir Res* 2010;**85**:75−90.
5. Tantillo C, Ding J, Jacobo-Molina A, Nanni RG, Boyer PL, Hughes SH, et al. Locations of anti-AIDS drug binding sites and resistance mutations in the three-dimensional structure of HIV-1 reverse transcriptase. Implications for mechanisms of drug inhibition and resistance. *J Mol Biol* 1994;**243**:369−87.
6. Ivetac A, McCammon JA. Elucidating the inhibition mechanism of HIV-1 non-nucleoside reverse transcriptase inhibitors through multicopy molecular dynamics simulations. *J Mol Biol* 2009;**388**:644−58.
7. Wang Z, Cherukupalli S, Xie M, Wang W, Jiang X, Jia R, et al. Contemporary medicinal chemistry strategies for the discovery and development of novel HIV-1 non-nucleoside reverse transcriptase inhibitors. *J Med Chem* 2022;**65**:3729−57.
8. Zhuang C, Pannecouque C, De Clercq E, Chen F. Development of non-nucleoside reverse transcriptase inhibitors (NNRTIs): our past twenty years. *Acta Pharm Sin B* 2020;**10**:961−78.
9. Jin X, Wang S, Zhao L, Huang W, Zhang Y, Pannecouque C, et al. Development of fluorine-substituted NH$_2$-biphenyl-diarylpyrimidines as highly potent non-nucleoside reverse transcriptase inhibitors: boosting the safety and metabolic stability. *Acta Pharm Sin B* 2023;**13**:1192−203.
10. Zhang X. Anti-retroviral drugs: current state and development in the next decade. *Acta Pharm Sin B* 2018;**8**:131−6.
11. Li G, Wang Y, De Clercq E. Approved HIV reverse transcriptase inhibitors in the past decade. *Acta Pharm Sin B* 2022;**12**:1567−90.
12. Sang YL, Pannecouque C, De Clercq E, Wang S, Chen FE. Picomolar inhibitor of reverse transcriptase featuring significantly improved metabolic stability. *Acta Pharm Sin B* 2023;**13**:3054−66.
13. Zhao LM, Wang S, Pannecouque C, De Clercq E, Piao HR, Chen FE. Discovery of novel biphenyl-substituted pyridone derivatives as potent non-nucleoside reverse transcriptase inhibitors with promising oral bioavailability. *Eur J Med Chem* 2022;**240**:114581.

14. Vitaku E, Smith DT, Njardarson JT. Analysis of the structural diversity, substitution patterns, and frequency of nitrogen heterocycles among U.S. FDA approved pharmaceuticals. *J Med Chem* 2014;**57**: 10257–74.

15. Kang D, Sun Y, Murugan NA, Feng D, Wei F, Li J, et al. Structure–activity relationship exploration of NNIBP tolerant region I leads to potent HIV-1 NNRTIs. *ACS Infect Dis* 2020;**6**:2225–34.

16. Ang CW, Tan L, Sykes ML, AbuGharbiyeh N, Debnath A, Reid JC, et al. Antitubercular and antiparasitic 2-nitroimidazopyrazinones with improved potency and solubility. *J Med Chem* 2020;**63**:15726–51.

17. Côté B, Burch JD, Asante-Appiah E, Bayly C, Bédard L, Blouin M, et al. Discovery of MK-1439, an orally bioavailable non-nucleoside reverse transcriptase inhibitor potent against a wide range of resistant mutant HIV viruses. *Bioorg Med Chem Lett* 2014;**24**:917–22.

18. Kim Y, Li CJ. Perspectives on green synthesis and catalysis. *Green Synth Catal* 2020;**1**:1–11.

19. Zhao LM, Pannecouque C, De Clercq E, Wang S, Chen FE. Structure-directed expansion of biphenyl-pyridone derivatives as potent non-nucleoside reverse transcriptase inhibitors with significantly improved potency and safety. *Chin Chem Lett* 2023:108261.

20. Wang Z, Yu Z, Kang D, Zhang J, Tian Y, Daelemans D, et al. Design, synthesis and biological evaluation of novel acetamide-substituted doravirine and its prodrugs as potent HIV-1 NNRTIs. *Bioorg Med Chem* 2019;**27**:447–56.

21. Pérez VE, Sánchez-Parra C, Serrano Villar S. Etravirine drug interactions. *Enferm Infecc Microbiol Clín* 2009;**27**(Suppl 2):27–31.

22. Kang D, Feng D, Sun Y, Fang Z, Wei F, De Clercq E, et al. Structure-based bioisosterism yields HIV-1 NNRTIs with improved drug-resistance profiles and favorable pharmacokinetic properties. *J Med Chem* 2020;**63**:4837–48.

23. Talwani R, Temesgen Z. Doravirine: a new non-nucleoside reverse transcriptase inhibitor for the treatment of HIV infection. *Drugs Today* 2020;**56**:113–24.

24. Garrido A, Lepailleur A, Mignani SM, Dallemagne P, Rochais C. hERG toxicity assessment: useful guidelines for drug design. *Eur J Med Chem* 2020;**195**:112290.

25. Kalyaanamoorthy S, Barakat KH. Development of safe drugs: the hERG challenge. *Med Res Rev* 2018;**38**:525–55.

26. Orkin C, Squires KE, Molina JM, Sax PE, Sussmann O, Lin G, et al. Doravirine/Lamivudine/Tenofovir Disoproxil Fumarate (TDF) *versus* Efavirenz/Emtricitabine/TDF in treatment-naive adults with human immunodeficiency virus type 1 infection: week 96 results of the randomized, double-blind, phase 3 DRIVE-AHEAD noninferiority trial. *Clin Infect Dis* 2021;**73**:33–42.

27. Zhou RL, Ju Z, Pannecouque C, Clercq E, Wang S, Chen FE. Structure-guided design of novel HEPT analogs with enhanced potency and safety: from isopropyl-HEPTs to cyclopropyl-HEPTs. *Eur J Med Chem* 2023;**246**:114939.